





## Article

# Sr Isotope, Major, and Trace Element Signatures in Karst Groundwaters

Anamaria Iulia Török<sup>1</sup>, Ana Moldovan<sup>1,\*</sup>, Claudiu Tănăselia<sup>1</sup>, Eniko Kovacs<sup>1,2</sup>, Ionuț Cornel Mirea<sup>3</sup>, Oana Teodora Moldovan<sup>4</sup> and Erika Andrea Levei<sup>1,\*</sup>

<sup>1</sup> Research Institute for Analytical Instrumentation Subsidiary of National Institute of Research and Development for Optoelectronics INOE 2000, 67 Donath, 400293 Cluj-Napoca, Romania

<sup>2</sup> Faculty of Horticulture, University of Agricultural Sciences and Veterinary Medicine, 3-5 Manastur, 400372 Cluj-Napoca, Romania

<sup>3</sup> Department of Geospeleology and Paleontology, Emil Racovita Institute of Speleology, Calea 13 Septembrie, 050711 Bucharest, Romania

<sup>4</sup> Cluj-Napoca Department, Emil Racovita Institute of Speleology, 5 Clinicilor, 400006 Cluj-Napoca, Romania

\* Correspondence: ana.moldovan@icia.ro (A.M.); erika.levai@icia.ro (E.A.L.)

**Abstract:** Natural and anthropogenic factors highly influence the concentration of major (Na, Mg, K, Ca) and trace (Sr, Ba, Mn, Li) elements, anions ( $\text{HCO}_3^-$ ,  $\text{NO}_3^-$ ,  $\text{SO}_4^{2-}$ ,  $\text{Cl}^-$ ), and Sr isotopic signatures. The current study identified the Sr isotopic signature in groundwaters from the Southern Carpathians and Apuseni Mountains karst areas of Romania and its relation to the water's chemistry. The Sr concentration ranged between 16.5 and 658  $\mu\text{g/L}$ , but in most groundwaters, it was below 200  $\mu\text{g/L}$ . A considerable spatial variation and a low temporal variation, with a slightly lower Sr concentration in the winter than in spring, were observed. The strong positive correlation of the Sr with Ca, Mg, K, and Na indicated the common source of these elements. The main source of the Sr in groundwaters was the dissolution of carbonates, especially calcite, and dolomite to a lesser extent. The  $^{87}\text{Sr}/^{86}\text{Sr}$  isotopic ratio ranged between 0.7038 and 0.7158. Generally, waters with a high Sr concentration and moderate  $^{87}\text{Sr}/^{86}\text{Sr}$  ratios indicated carbonate dissolution, whereas samples with low Sr concentrations and high  $^{87}\text{Sr}/^{86}\text{Sr}$  ratios suggested the dissolution of silicates.

**Keywords:** groundwater; Sr isotopic ratio; major elements; spring water



**Citation:** Török, A.I.; Moldovan, A.; Tănăselia, C.; Kovacs, E.; Mirea, I.C.; Moldovan, O.T.; Levei, E.A. Sr Isotope, Major, and Trace Element Signatures in Karst Groundwaters. *Water* **2023**, *15*, 1431. <https://doi.org/10.3390/w15071431>

Academic Editor: Domenico Cicchella

Received: 15 February 2023

Revised: 18 March 2023

Accepted: 3 April 2023

Published: 6 April 2023



**Copyright:** © 2023 by the authors. Licensee MDPI, Basel, Switzerland. This article is an open access article distributed under the terms and conditions of the Creative Commons Attribution (CC BY) license (<https://creativecommons.org/licenses/by/4.0/>).

## 1. Introduction

Karst areas are essential contributors to the global freshwater supply, due to their complex porous mediums with highly soluble rocks that allow for groundwater flow-through and retention [1]. At the same time, because of their complex hydrology and geology, karst systems are very susceptible to changes, particularly to those that are induced by humans (contamination and land use change), which may have an impact on both the discharge and the water quality [2].

The composition of the groundwater in karst areas is influenced by various natural factors, such as the complex setting of the lithological and tectonic structure, geomorphology, meteorology, and hydrology, as well as by anthropic factors, such as water abstraction and pollution [2,3]. The anthropogenic contaminants from the spring's recharge area percolate into the karst system, where they reside for different periods of time, suffer changes through retention or microbial degradation, and are finally washed out in the springs [3]. The influence of the relief's topography on the groundwater depth, flow, and transport is still uncertain. Some studies have reported a relation between the topography, flow, and transport of groundwater [4,5], while other studies have showed that topography is merely one of the key elements influencing the groundwater structure, together with geology (through its layers) and climate (through recharge) [6,7]. The distribution of solutes in groundwater may be influenced by this topography, but the chemistry of these solutes

largely depends on the lithology of the rocks, meteorological conditions, and salt water discharge [8]. The recharge with surface water is favored by a thin epikarst and the presence of sinkholes and conduits, while the mix of water from different sources that reaches the spring outlet is controlled by the meteoric inputs [9]. Gong et al. [10] studied the origin and evolution of solutes in groundwater from an alpine area and a valley plain, concluding that altitude, water–rock interaction, precipitation, ground ice meltwater, weathering, ion exchange, and adsorption affected the chemical characteristics of the water. Although meteorology has a critical role in hydrology, the specific mechanistic interdependence of the climatic, hydrologic, and geochemical processes in karst systems is far from being understood [11].

Strontium (Sr) is a naturally occurring alkaline element present in the environment in the form of four stable isotopes:  $^{84}\text{Sr}$  (<1%),  $^{86}\text{Sr}$  (~10%),  $^{87}\text{Sr}$  (~7%), and  $^{88}\text{Sr}$  (~82%) [12–14]. The  $^{87}\text{Sr}/^{86}\text{Sr}$  ratio is highly influenced by a mineral's solubility and the age and chemical composition of the bedrock, and varies widely, both on local and regional scales [15,16]. The most important Sr-bearing minerals are silicates such as feldspars, biotite, and muscovite, and carbonates such as calcite, dolomite, and aragonite [17]. Generally, Sr is released faster from reactive minerals such as calcite than from recalcitrant minerals such as silicates. Due to its similar geochemical behavior with Ca, Sr can substitute Ca in minerals [18].

In karst areas, the isotopic signature of Sr in groundwater, especially the  $^{87}\text{Sr}/^{86}\text{Sr}$  isotopic ratio, is a commonly used tracer of weathering, water–rock interactions, and the associated geochemical processes in natural environments, particularly in Ca-bearing mineral dissolution, as well as in water mixing and flow paths [15,19–22].

The water–rock interaction and physical and chemical processes such as ion exchange, mineral solubility, precipitation, and flow characteristics influence not only the Sr concentration but also its isotopic signature. Previous studies have reported that these Sr concentrations are often regulated by the local rock types and the rock–water interaction [23]. An increase in the Sr concentration and a decrease of the  $^{87}\text{Sr}/^{86}\text{Sr}$  ratio in the recharge to discharge area was reported by Wang et al. [18]. The influences of dolomite, limestone dissolution, and rock weathering on the Sr concentrations, anthropogenic activities, and  $^{87}\text{Sr}/^{86}\text{Sr}$  ratios of groundwaters from karst areas were reported by Pu et al. [24] and Jiang [25]. The groundwater flow and water–rock dynamics in karst areas of Italy and Slovenia were studied using Sr isotope ratios combined with geochemical analyses [26]. McKay et al. [27] identified several flow pathways and the saline water intrusion based on the Sr isotope ratios and ion geochemistry in the Yucatan Peninsula, Mexico.

A hydrochemical model based on the reservoir type, time series analysis, and a dual flow system simulation was developed by Zhang et al. to assess the dissolution of carbonate rocks [9]. Based on experimental data and modeling, Charlier et al. built a conceptual model for water infiltration and dissolved organic carbon transport [28]. A study conducted in two water basins in the USA investigated the water–rock interaction and mixing of various groundwaters through the use of Sr isotopes, showing their effectiveness in groundwater source localization and dynamics, the identification of rock types, and water mixing proportions [29]. Isotopes and geochemical tracers, coupled with hydrodynamics, were used to develop a model for groundwater circulation in the Lez karst system, France. The results showed that long-residence-time groundwaters have high  $\text{Cl}^-$  concentrations, as well as high Sr/Ca, Mg/Ca, and  $^{87}\text{Sr}/^{86}\text{Sr}$  ratios [30]. However, the development of a conceptual model of the processes controlling the solute evolution in large and heterogeneous karst systems, by combining the interpretation of the isotopic composition with the chemistry of the major elements, remains a research challenge.

To our best of our knowledge, there are no data on the isotopic signatures of Sr in groundwaters from the karst areas in Romania. Additionally, despite the high number of interdisciplinary studies on karst systems, the mechanisms that control the groundwater chemistry in the karst areas of Romania are not deconvoluted. In this context, the objectives of the study are: (i) to identify the Sr isotopic signature in the groundwaters from the karst areas located in the Southern Carpathians and Apuseni Mountains, Romania, and (ii) to

assess the influence of mineral weathering on the regional variation of Sr and its isotopic signature. The data obtained by the present study can be used as baseline information for further geochemistry research.

## 2. Materials and Methods

### 2.1. Study Area, Sampling and Sample Preparation

In Romania, karst areas cover about 5500 km<sup>2</sup> (~2.3% of the country area) and are located mainly in the Carpathian Mountains and along the Black Sea coast [31]. In total, 10 natural springs located in the karst area of the Southern Carpathians (SCP) and 14 natural springs located in the karst area of the Apuseni Mountains (APS), Romania (Figure 1), were studied. These small springs are only used by the locals, are distributed in different geographical and geological units, and to the best of our knowledge, there are no data on their hydrology or local geological profiles. The main features of these SCP and APS karst areas are presented in Table 1. More details and geologic maps on the studied areas are provided by Orășeanu [32], Goran et al. [33], Hoaghia et al. [34], and Moldovan et al. [35]. The groundwater from each spring was collected in the winter of 2020 (W20), spring of 2020 (S20), winter of 2021 (W21), and spring of 2021 (S21).

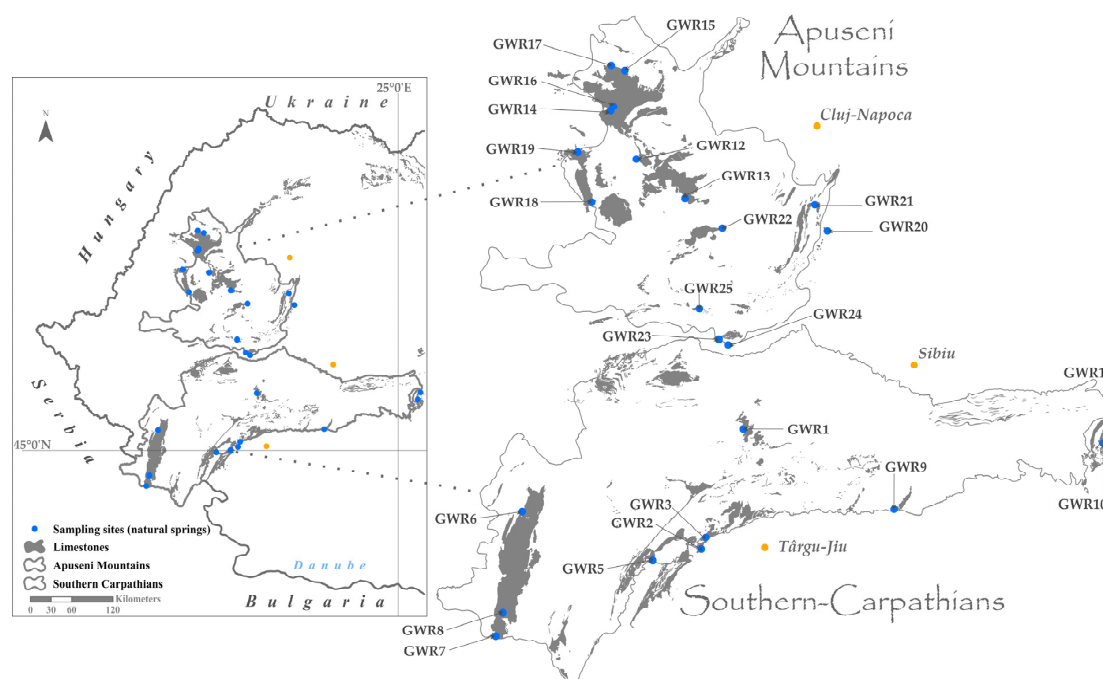


**Figure 1.** Springs (GWR) located in the Southern Carpathians (SCP) and the Apuseni Mountains (APS) karst areas.

**Table 1.** Characteristics of the study area.

	<b>Southern Carpathians (SCP)</b>	<b>Apuseni Mountains (APS)</b>
Sampling sites	GWR1-GWR3, GWR5-GWR11	GWR12-GWR25
Geology	Limestones, sandstones	Limestones, dolomites, conglomerates, crystalline schists, crystalline limestones, dolostones
Type of aquifers	Local or discontinuous aquifers	Local or discontinuous aquifers
Type of climate	Moderate continental/Sub-Mediterranean climate	Cold continental climate
Main land use	Non-irrigated arable land, broad-leaved forests, and pastures	Non-irrigated arable land, broad-leaved and mixed forests

The samples were collected in pre-cleaned, 500 mL, high-density polyethylene (HDPE) bottles and transported to the laboratory in ice-packed cool boxes. In the laboratory, the samples were filtered through 0.45- $\mu\text{m}$  cellulose acetate membrane filters, acidified to  $\text{pH} < 2$  with ultrapure 60%  $\text{HNO}_3$  (Merck, Darmstadt, Germany), and stored at  $4^\circ\text{C}$  until analysis. The field and laboratory blanks were prepared the same as the samples, using ultrapure water (Elga Veolia, High Wycombe, UK).

## 2.2. Analysis

All the reagents were of an analytical grade and were used without any further purification. Ultrapure water (Elga Veolia, High Wycombe, UK) was used for all the dilutions and for the preparation of the standard solutions. The Ca, Na, Mg, and K concentrations in the groundwater were measured using an Optima 5300 DV inductively coupled plasma optical emission spectrometer (ICP-OES, Perkin Elmer, Waltham, MA, USA), while the Sr, Ba, Mn, and Li concentrations were measured using an ELAN DRC II inductively coupled mass spectrometer (ICP-MS, Perkin Elmer SCIEX, ON, Canada). The bicarbonates ( $\text{HCO}_3^-$ ) were determined by titration with 0.1 N HCl in the presence of bromocresol green. The anions ( $\text{Cl}^-$ ,  $\text{NO}_3^-$ ,  $\text{SO}_4^{2-}$ ) were determined via ion chromatography, using a 761 IC compact ion chromatograph (Metrohm, Herisau, Switzerland). A multi-element Calibration Standard 3 (Perkin Elmer Pure Plus, Waltham, MA, USA) was used for the calibration of the spectrometers, while standard solutions of 1000 mg/L  $\text{Cl}^-$ , 1000 mg/L  $\text{NO}_3^-$ , and 1000 mg/L  $\text{SO}_4^{2-}$  (Certipur, Supelco, Merck, Darmstadt, Germany) were used for the ion chromatograph calibration. The accuracy of the measurements was tested using the IC Multi-Element standard 1 (Certipur, Supelco, Merck, Darmstadt, Germany) for the anions and the 1643f NIST-Trace elements in water certified reference material (National Institute of Standards and Technology, Gaithersburg, MD, USA) for the metals. Each sample was analyzed in triplicate. The average recoveries ranged between 93–104% for the metals and between 89–102% for the anions. The analytical precision for the measurements of the cations and anions was assessed by the ionic balance error, which was within  $\pm 10\%$ . The turbidity (TU) of the spring waters was measured by a Turb 555 IR turbidimeter (WTW, Weilheim, Germany).

In the lab blanks, as well as in most of the field blanks, the concentrations of the elements were below the limit of detection (LOD), or were negligible compared to the concentrations that were measured in the samples. The LOD (Table 2) was calculated as three times the ratio between the standard deviation of the signal of 10 reagent blank measurements and the slope of the calibration curve [36].

**Table 2.** Limit of detection (LOD) of elements in groundwater.

Element	$\text{Cl}^-$	$\text{NO}_3^-$	$\text{SO}_4^{2-}$	Ca	Na	Mg	K	Sr	Ba	Mn	Li
Unit	mg/L	mg/L	mg/L	mg/L	mg/L	mg/L	mg/L	$\mu\text{g/L}$	$\mu\text{g/L}$	$\mu\text{g/L}$	$\mu\text{g/L}$
LOD	0.20	0.20	0.20	0.004	0.008	0.009	0.003	0.13	0.16	0.13	0.12

The expanded uncertainty (U) was calculated by multiplying the combined standard uncertainty with the coverage factor ( $k = 2$ ) for a level of confidence of 95%. The combined standard uncertainty was calculated as the root sum of squares of the individual uncertainties [37]. The expanded uncertainty was below 10% for all the elements.

## 2.3. Strontium Isotopy

The strontium isotopic determinations were conducted using an iCAP TQ inductively coupled plasma mass spectrometer (ICP-MS, ThermoFisher Scientific, Bremen, Germany), equipped with a triple quadrupole system for ion discrimination and a single detector for ion collecting. A dwell time of 0.02 s for  $^{87}\text{Sr}$  and  $^{86}\text{Sr}$  was set to counteract the plasma variation, while maintaining it proportional to the Sr natural abundance and enabling the detector to remain in ion counting mode, which is more precise than the analog

(Faraday) mode, or a transient, calibrated mode. A single channel was used for all the isotope readings (peak-hopping mode), while for every measurement, 500 sweeps and 5 replicates were performed for each sample. The spectrometer was used in the High Matrix configuration, with a nickel sampler and skimmer cones. The quartz spray chamber was kept constant at 2.7 °C by a built-in Peltier device and a concentric nebulizer was used for all the measurements. The Qtegra software (v. 2.10.3324.131), provided by the manufacturer, was used for the data acquisition. Before each sample batch, the instrument was calibrated for high sensitivity, low noise, low oxide levels, and low double-ionized species, using the methods that were available in the software supplied by the manufacturer. To remove any potential Rb interference, oxygen was used in the ICP-MS collision cell, which reacted with the Sr isotopes, thus shifting the mass read on the detector to 102 ( $^{86}\text{Sr}^{16}\text{O}^+$ ) and 103 ( $^{87}\text{Sr}^{16}\text{O}^+$ ) [38]. Any potential  $^{103}\text{Rh}$  interferences were rejected on the first quadrupole, set to allow passage only for the strontium isotope masses, and any potential  $^{87}\text{Rb}$  interference ions were rejected on the third quadrupole, set to allow passage only for strontium–oxygen dimers, with masses of 102 and 103. The main instrument parameters are presented in Table 3.

**Table 3.** Instrumental parameters of iCAP TQ ICP-MS.

Parameter	Value	Parameter	Value
Argon flow	0.92 mL/min	Q3 bias	−1.0003 V
Oxygen flow (CRC)	0.35 mL/min	Focus lens	20.10 V
Extraction lens	−132.1 V	RAPID lens	−380 V
Spray chamber temperature	2.7 °C	Plasma power	1550 W
Q1 focus lens	−1 V	Cool flow	14 L/min
QCell bias	−2.01 V	Auxiliary flow	0.8 L/min

For the isotopic ratio measurements, a bracketing calibration was performed, using NIST 987 standard reference material that was dissolved in 3%  $\text{HNO}_3$  and diluted to a concentration of 20  $\mu\text{g/L}$  Sr, to offer the best sensitivity while not saturating the detector or causing memory effects. The signal of the blank was subtracted from the signal of the subsequently measured samples. The obtained values for the NIST SRM 987 have a relative standard deviation of 102.8% for  $^{87}\text{Sr}/^{86}\text{Sr}$ , which indicates a good accuracy of the determination of the Sr isotopic ratios.

The relationship between the strontium isotope ratios was expressed using a  $\epsilon\text{Sr}$  notation (Equation (1)), where the  $^{87}\text{Sr}/^{86}\text{Sr}$  in the sample was normalized to the globally uniform,  $^{87}\text{Sr}/^{86}\text{Sr}$ , of present-day seawater (0.709169) [13,39,40].

$$\epsilon\text{Sr} = \left( \frac{(^{87}\text{Sr}/^{86}\text{Sr})_{\text{sample}}}{(^{87}\text{Sr}/^{86}\text{Sr})_{\text{seawater}}} - 1 \right) \times 10^4 \quad (1)$$

### 3. Results and Discussion

#### 3.1. Strontium

The Sr concentration (Figure 2) was below 200  $\mu\text{g/L}$  in all the groundwaters from the SCP region and most of the groundwaters from the APS region in both years, in winter and spring. Sr concentrations above 200  $\mu\text{g/L}$  were measured in GWR20 (381–658  $\mu\text{g/L}$ ), GWR23 (366–538  $\mu\text{g/L}$ ), and GWR24 (251–324  $\mu\text{g/L}$ ) from the APS region, in both years and both seasons. The average Sr concentration was more than twice higher in the APS region (137  $\mu\text{g/L}$ ) than in the SCP region (52.6  $\mu\text{g/L}$ ), but the median Sr concentrations (68.9  $\mu\text{g/L}$  in APS and 44.6  $\mu\text{g/L}$  in SCP) were comparable.

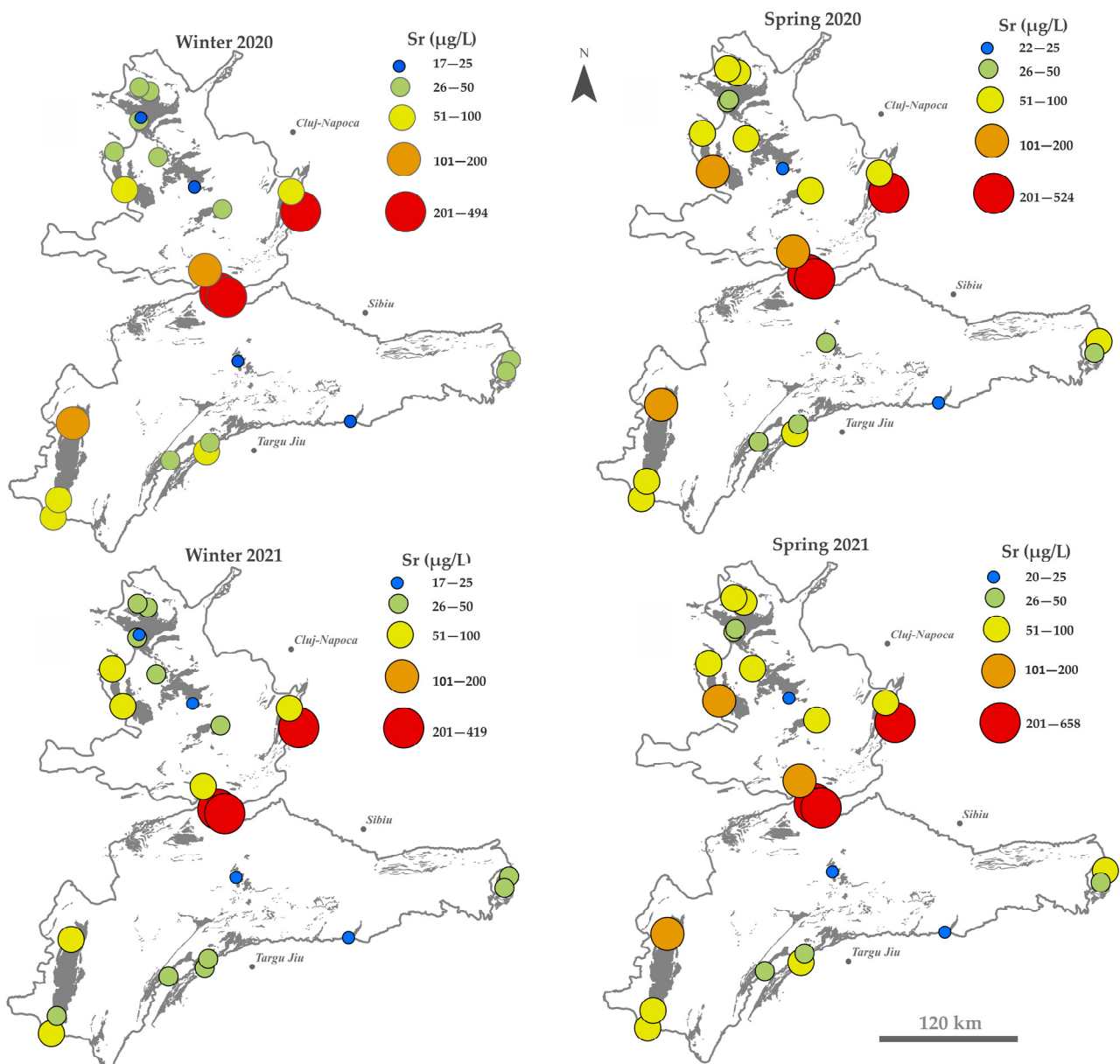


**Figure 2.** Concentration of Sr ( $\mu\text{g/L}$ ) in groundwaters from the Southern Carpathians (SCP) and Apuseni Mountains (APS) karst areas.

Generally, the Sr concentrations were comparable in the same seasons of 2020 and 2021, and were slightly lower in winter than in spring (Table S1). However, in some samples from the APS region (GWR18, GWR20, GWR23, GWR24, and GWR25), a higher variability of the Sr concentrations was noticed. In all samples and both years, the Sr concentrations were well below the health reference level ( $1500 \mu\text{g/L}$ ) that is set for drinking water [41].

The dissolutions of Sr-bearing minerals (silicates and carbonates), meteoric water, and, to a smaller extent, anthropogenic inputs (fertilizers and deicing salts) are the main Sr sources in groundwater [24,39,42–44]. As both the SCP and APS regions are located inland, far from marine influence, in rural areas, the Sr input from human activities and atmospheric deposition is low. The variation in the Sr concentration among the samples may be attributed to the influence of the aquifer type and geological setup. Strontium is considered to be highly soluble and mobile and is mainly released through weathering processes [45]. Ultrabasic rocks and sandstones have generally low Sr contents, while carbonates, evaporites, granites, and aragonitic rocks have high Sr contents [45–47]. Among

carbonates, the highest Sr contents (up to 10,000 mg/kg) are found in aragonite and carbonate fossils [47]. The highest Sr concentrations in aquifers across the United States were found by Musgrove in unconsolidated sand and gravel aquifers, and they were attributed to irrigation and the evaporative concentration of dissolved constituents, in combination with the lithological or anthropogenic Sr inputs [45]. Based on a study conducted in western Europe, the median value reported for the Sr in stream water was 110  $\mu\text{g/L}$ , with the highest values being found in Italy, Spain, and northern France (higher than 14 mg/L) [48]. The median Sr concentration in the groundwaters (53.4  $\mu\text{g/L}$ ) that were measured in the present study was comparable with the European median value, but much lower than those reported in Denmark (1.17 mg/L) [48,49].

### 3.2. Groundwater Chemistry

As expected, the dominance of the alkaline earths (Ca+Mg) over the alkali elements (Na+K), and of  $\text{HCO}_3^-$  over the other anions, was observed in all the samples (Tables S1 and S2). This dominance is specific to the groundwaters in karst areas and is attributed to the nature and composition of the bedrock that controls the groundwater's mineralization [46]. Generally, the Ca, Na, K, and Mg concentrations in the groundwater (Figure 3 and Table S1) were comparable in the two analyzed years (2020 and 2021) and seasons (winter and spring).

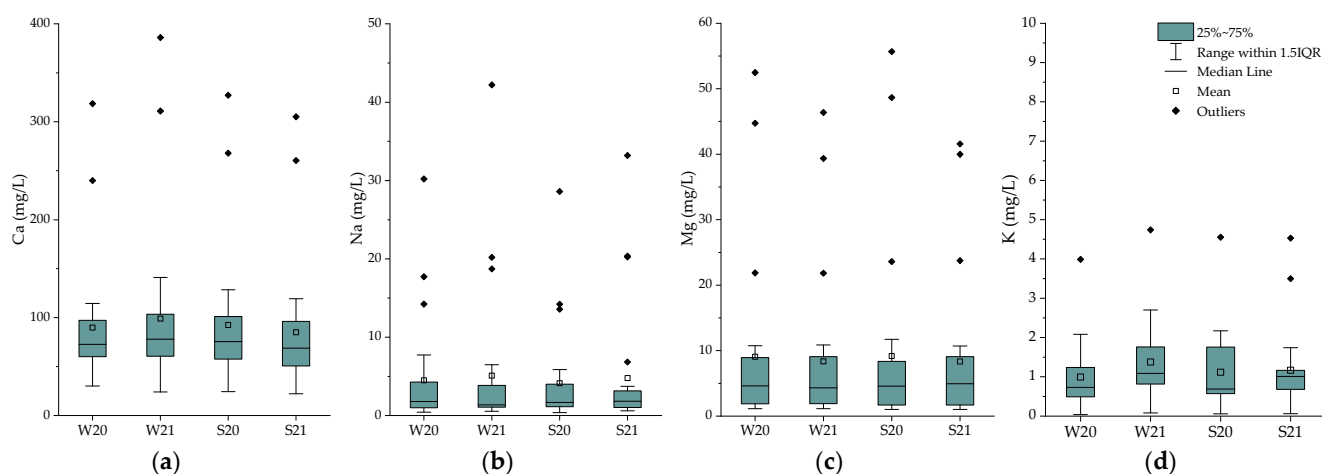


**Figure 3.** Boxplot of Ca (a), Na (b), Mg (c), and K (d) concentrations (mg/L) in groundwaters in winter (W) and spring (S) seasons of 2020 (20) and 2021 (21).

In the APS region, the concentrations of all the major elements were higher than in the SCP region. The highest concentrations of Ca, Mg, and K were observed in GWR23, while the highest Na concentration was in GWR20. The Ca concentration varied among the sampling sites and ranged between 24.5 and 327 mg/L in 2020, and between 22.2 and 386 mg/L in 2021. The Ca concentrations were below 100 mg/L in most of the samples. Ca concentrations above 200 mg/L were found only in GWR23 (305–386 mg/L) and GWR24 (240–311 mg/L), located in the APS region. The average Ca concentration was slightly higher in the APS region (104 mg/L) than in the SCP region (73.6 mg/L), but the median Ca concentrations in the two regions were similar (75.0 mg/L in APS and 74.8 mg/L in SCP). The Na concentration was below 10 mg/L in all the samples, except for GWR6 (14.2–20.4 mg/L) in the SCP region and GWR20 (28.6–42.2 mg/L) and GWR23 (14.2–20.3 mg/L) in the APS region. Similar to Ca, the average Na concentration in the APS region (5.46 mg/L) was higher than that in the SCP region (3.45 mg/L), but the median concentrations were comparable (1.77 mg/L in APS and 1.68 mg/L in SCP). The Mg concentrations varied between 1.01 and 55.7 mg/L, and between 1.02 and 46.4 mg/L, in 2020 and 2021, respectively. Likewise, the majority of the samples had Mg concentrations below 10 mg/L, with concentrations above 10 mg/L being obtained in a few samples from

the APS region (GWR18, GWR19, GWR23, and GWR24). The highest Mg concentrations were measured in GWR23 (41.6–55.7 mg/L), followed by GWR24 (39.4–48.7 mg/L) from the APS region. The average Mg concentration was three times higher in the groundwater from the APS region (12.3 mg/L) than that from the SCP region (3.75 mg/L), while the median Mg concentration was twice higher in the APS region (6.06 mg/L) than in the SCP (3.20 mg/L) region. Low K concentrations (<2.0 mg/L) were found in most of the samples, with the highest concentration in GWR23 (3.99–4.74 mg/L), located in the APS region. The average K concentration was twice higher in the APS region (1.44 mg/L) than in the SCP region (0.79 mg/L), and the median was also slightly higher (1.09 mg/L) in the APS region than in SCP region (0.71 mg/L).

The concentrations of the Ba (4.5–760 µg/L), Mn (0.06–128 µg/L), and Li (0.10–67.9 µg/L) (Figure 4 and Table S1) that were measured in 2020 and 2021 were comparable, as well as those that were measured in the spring and winter. With a few exceptions, the Ba, Mn, and Li concentrations in the groundwaters were less than 50, 3, and 5 µg/L, respectively. Concentrations of Ba above 50 µg/L were measured in GWR18 (82–114 µg/L) GWR23 (567–759 µg/L), and GWR24 (131–144 µg/L), of Mn above 3 µg/L in GWR23 (91.1–128 µg/L), GWR24 (27.6–45.4 µg/L), and GWR7 (12.6–15.5 µg/L), and of Li above 5 µg/L in GWR23 (54.6–67.9 µg/L) and GWR24 (13.0–16.8 µg/L Li). As all the alkaline earth elements have similar geochemical behavior, the Ba and Sr are able to stoichiometrically substitute the Ca and Mg in carbonates [46].

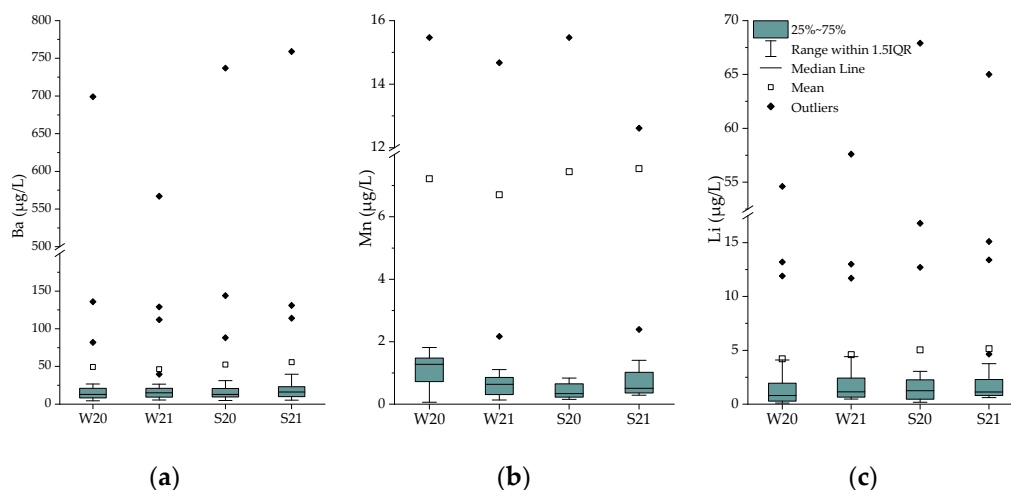


**Figure 4.** Boxplot of Ba (a), Mn (b), and Li (c) concentrations (µg/L) in groundwaters in winter (W) and spring (S) seasons of 2020 (20) and 2021 (21).

The average concentrations of Ba (79.7 µg/L), Mn (10.9 µg/L), and Li (7.46 µg/L) in the APS region were much higher than those in the SPC region (10.8 µg/L Ba, 2.06 µg/L Mn, and 0.962 µg/L Li), and the median concentrations of Ba and Li were about twice higher in the APS region (18.7 µg/L Ba and 1.36 µg/L Li) than in the SCP region (9.7 µg/L Ba and 0.81 µg/L Li), yet the median Mn concentrations were comparable (0.536 and 0.658 µg/L).

Strong positive correlations of the Sr ( $r = 0.62–0.88$ ) with the Ca, Mg, K, and Na were noticed in both years and both seasons, suggesting the common source of these elements. Previous studies have also reported positive correlations between Sr and major elements such as Ca, Mg, K, and Na [24,45]. Strong correlations between the Ca, Ba, and Sr in the groundwater from karst areas have also been reported, as these elements result mainly from the dissolution of carbonates, especially limestone [50,51].

The  $\text{HCO}_3^-$  concentration was similar in the two regions and ranged between 134 and 354 mg/L in the SCP region, and between 124 and 415 mg/L in the APS region. However, in GWR23 and GWR24, the  $\text{HCO}_3^-$  concentration was one order of magnitude higher (1166–1610 mg/L). A very strong ( $r > 0.8$ ) positive correlation of  $\text{HCO}_3^-$  with Ca, Mg, Ba, Mn, and Li, and strong ( $0.65 < r < 0.8$ ) positive correlation of  $\text{HCO}_3^-$  with K and Sr



( $r = 0.66\text{--}0.85$ ) were found. These correlations suggest that all the elements result mainly from the dissolution of carbonate-type minerals.

The  $\text{Cl}^-$  concentration ranged between 0.57 and 66 mg/L in the SCP region, between 0.53 and 100 mg/L in the APS region, and was below the guideline value (250 mg/L) established by the Drinking Water Directive [52] in all the samples. The highest  $\text{Cl}^-$  concentration in the APS region was measured in GWR20 (86.0–100 mg/L), while in the SCP region it was in GWR6 (33.0–66.0 mg/L). The moderate positive correlation of  $\text{Cl}^-$  with Sr ( $r = 0.53\text{--}0.70$ ) suggests that, besides carbonate dissolution, Sr may result also from the dissolution of chlorides. The presence of nitrates in groundwater is primarily associated with human and agricultural activities [53]. In the current study, all the groundwaters had low  $\text{NO}_3^-$  concentrations, being far below the guideline value (50 mg/L) established by the Drinking Water Directive [52]. The concentrations of  $\text{SO}_4^{2-}$  were below 40 mg/L in all the samples, being one order of magnitude below the guideline for drinking water (250 mg/L). Like Sr, the highest values of  $\text{Cl}^-$  and  $\text{SO}_4^{2-}$  were observed in the case of GWR20 (86.0–100 mg/L  $\text{Cl}^-$  and 34.0–40.0 mg/L  $\text{SO}_4^{2-}$ ). While the presence of  $\text{Cl}^-$  and  $\text{SO}_4^{2-}$  may be related to silicate weathering and the dissolution of halite and sulfate minerals, the presence of  $\text{NO}_3^-$  is a sign of anthropogenic pollution sources, such as  $\text{NO}_3^-$  fertilizers and septic tanks.

The TU and flow rates are natural tracers of groundwater hydrology [54]. With a few exceptions, the TU was below 4 NTU. In the APS region, TUs above 4 NTU were found in GWR12 in the winter (8.8 NTU) and spring (10.2 NTU) of 2021, in GWR18 in the winter of 2020 (8.1 NTU), and in GWR1 in the winter of 2021 (5.70 NTU). The flow rate greatly varied both among the sampling sites and the sampling seasons. The lack of correlation between the flow rate and the studied parameters may be a sign of a non-heterogeneous composition of the karst water, a variation among the charge and discharge cycles of the aquifer, and the possible multiple flow paths of the water from the aquifer to the groundwaters [55].

The groundwater hydrogeochemical facies were assessed based on the proportions of the major ions using the Piper diagram, and revealed that all of the groundwaters had similar Ca-Mg- $\text{HCO}_3^-$  facies (Figure 5). The influence of rock weathering on the water chemistry was given by the dominance of the alkaline earth metals ( $\text{Ca}^{2+} + \text{Mg}^{2+}$ ) over the alkali elements ( $\text{Na}^+ + \text{K}^+$ ), and the weak acids ( $\text{HCO}_3^-$ ) over the strong acids ( $\text{Cl}^- + \text{SO}_4^{2-}$ ). There were no noticeable changes in the hydrochemical facies between the sampling seasons in all the groundwater sources, indicating that the major ions were of natural origin.

The Ca/Mg molar ratio in the groundwater ranged between 3.40 and 44.3 in the SCP region and between 1.26 and 46.2 in the APS area, with low seasonal or annual fluctuations. The high variability of the Ca/Mg molar ratio between the groundwater samples indicates various Ca and Mg sources, including carbonates and silicates, as well as a different residence time of the water in the karst system [11]. The Ca/Ca+Mg molar ratio of 0.5 corresponds to the dissolution of dolomite, while a molar ratio of 1 corresponds to calcite dissolution [56]. The Ca/Ca+Mg ratios varied between 0.77 and 0.98 for the SCP region and between 0.56 and 0.98 for the APS region, with only very small annual and seasonal differences. In the current study, the high values of the Ca/Ca+Mg molar ratio indicate the predominance of calcite dissolution over dolomite dissolution in both areas.

To explore the main lithological sources of the elements in the water, scatterplots of different element combinations were drawn [53,56,57]. As the samples fall well below the equiline of Ca+Mg versus Na+K (Figure 6a), it is suggested that the dominant source of the major ions in the water is carbonate dissolution. The Ca/Mg versus Mg plot (Figure 6b) shows a decrease in the Ca/Mg molar ratio with an increase in the Mg concentration, suggesting that, in the samples with high Mg concentrations, dolomite weathering is the main source of the Ca and Mg. Generally, a low Ca/Mg molar ratio is attributed to the weathering of silicates and/or dolomite, while high molar ratios can result from calcite weathering [56].

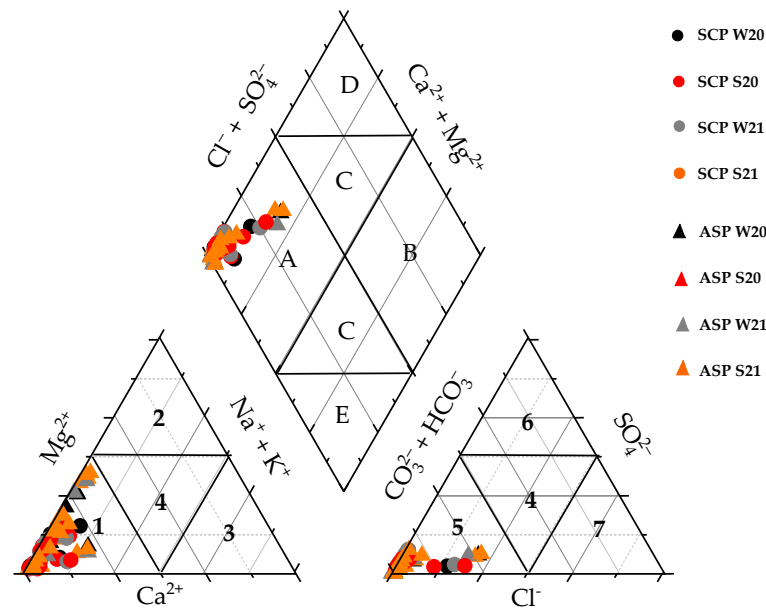


**Figure 5.** Piper diagram illustrating the water facies (A—Magnesium bicarbonate type, B—Sodium chloride type, C—Mixed type, D—Calcium chloride type, and E—Sodium bicarbonate type; 1—Calcium type, 2—Magnesium, 3—Sodium and potassium, 4—Non dominant type, 5—Bicarbonate type, 6—Sulphate type, and 7—Chloride type).

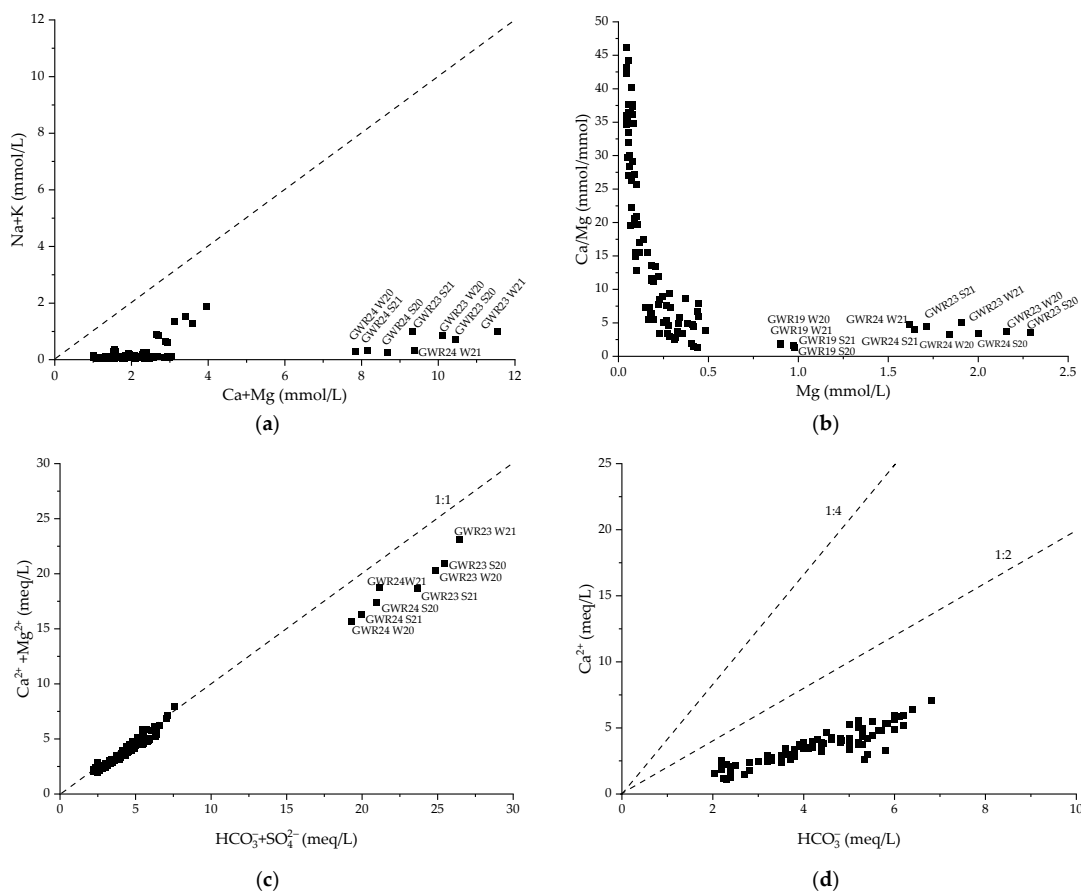


**Figure 6.** Scatter plots showing possible sources of elements in the different seasons in the two studied regions: (a) Na+K versus Ca+Mg, (b) Ca/Mg versus Mg, (c)  $\text{HCO}_3^- + \text{SO}_4^{2-}$  versus  $\text{Ca}^{2+} + \text{Mg}^{2+}$ , and (d)  $\text{HCO}_3^-$  versus  $\text{Ca}^{2+}$ .

The ratio of  $(\text{Ca}^{2+} + \text{Mg}^{2+})$  to  $(\text{HCO}_3^- + \text{SO}_4^{2-})$  in most of the samples was around 1, indicating carbonate dissolution, while in a few samples with a ratio below 1 (Figure 6c), the presence of silicate weathering impacted the chemistry of  $\text{Ca}^{2+}$  and  $\text{Mg}^{2+}$ . The  $\text{Ca}^{2+}$  to  $\text{HCO}_3^-$  ratio for the groundwater developed in dolomite and calcite aquifers is typically between 1/4 and 1/2. Nonetheless, all the samples (Figure 6d) fell below the 1/2 ratio, indicating that  $\text{Ca}^{2+}$  was removed from the water through reactions such as cation exchange [53].

In general, Ba and Sr occur in various minerals with different dissolution rates. Usually, Sr substitutes Ca and Mg, and to a lesser extent K, while Ba mainly substitutes K [39]. The Ba/Sr molar ratio was very low ( $<1$ ) in the groundwater samples, in both years and seasons, except for GWR23 in January 2021, where the ratio was slightly higher (Table S3). The Ca/Sr molar ratio did not vary with the year or season, although it varied from sample to sample (Table S3).

### 3.3. Sr Isotopic Ratio

The  $^{87}\text{Sr}/^{86}\text{Sr}$  ratio varied from sample to sample, in the range of 0.7038–0.7158 (Figure 7 and Table S4). A high variation of the  $^{87}\text{Sr}/^{86}\text{Sr}$  ratio was observed in the case of the groundwaters from GWR2, GWR3, and GWR9 in the SCP region, and GWR13, GWR17, GWR21, GWR22, and GWR24 in the APS region. Generally,  $^{87}\text{Sr}/^{86}\text{Sr}$  ratios above 0.7100 were associated with low Sr concentrations, indicating silicate dissolution, while ratios lower than 0.7080 were associated with high Sr contents, suggesting carbonate dissolution [58,59]. In the present study, only GWR1, GWR2, and GWR3 from the SCP region showed  $^{87}\text{Sr}/^{86}\text{Sr}$  ratios higher than 0.7100 and relatively low Sr concentrations, suggesting that Sr may originate from silicate dissolution. In the APS region, the  $^{87}\text{Sr}/^{86}\text{Sr}$  ratios only occasionally exceeded 0.7100. The  $^{87}\text{Sr}/^{86}\text{Sr}$  ratios between 0.7057 and 0.7079 were attributed to the Sr dissolution in the Cretaceous granite area in hot spring waters from South Korea [43]. It has been previously reported that  $^{87}\text{Sr}/^{86}\text{Sr}$  ratios of 0.707–0.709 result from carbonate recycling [60] and that the dissolution of carbonate sediments results in low  $^{87}\text{Sr}/^{86}\text{Sr}$  ratios [61].

In the present study,  $^{87}\text{Sr}/^{86}\text{Sr}$  ratios lower than 0.708 were observed in the cases of GWR5–GWR8 in the SCP region and GWR25 in the APS region, for both seasons in both years, while in GWR14, GWR15, GWR17, and GWR20, only in the case of the winter season (for the years 2020 and 2021). Generally, the Sr concentration in the groundwaters from karst areas is controlled by the amount of rainfall, the dissolution of minerals containing Sr, and anthropogenic inputs, while the  $^{87}\text{Sr}/^{86}\text{Sr}$  ratio is controlled only by the water–rock interaction and does not depend on the meteoric inputs, nor on other external factors [62,63]. In the current study, the moderately negative correlation between the  $^{87}\text{Sr}/^{86}\text{Sr}$  and Sr (with  $r$  values between  $-0.42$  and  $-0.71$ ) indicates that the Sr chemistry in the groundwaters from the SCP region is controlled by the water–rock interaction, and to a lesser extent, by other factors, such as the influx of meteoric or surface water. The poor correlation between the  $^{87}\text{Sr}/^{86}\text{Sr}$  and Sr ( $r$  values between  $-0.04$  and  $-0.42$ ) in the APS region suggests the dominance of external processes over the water–rock interaction in defining the Sr chemistry.

The  $^{87}\text{Sr}/^{86}\text{Sr}$  ratio of the Sr originating from silicate dissolution is higher (0.716–0.720) than that originating from calcite (0.7075–0.7080) and dolomite (0.7080–0.7100). In our case, most of the groundwater samples lay in the carbonate dissolution area, and few were in the transition area between silicates and carbonates [39]. It can be observed (Figure 8) that groundwaters with a high Sr concentration (GWR20, GWR23, and GWR24 from the APS region) and moderate  $^{87}\text{Sr}/^{86}\text{Sr}$  ratios are clearly separated from the other samples and are characterized by the carbonates' dissolution, whereas in the samples with low Sr concentrations and high  $^{87}\text{Sr}/^{86}\text{Sr}$  ratios ( $>0.7100$ ), the Sr originates from the dissolution of both silicates and carbonates (GWR1–3 in the SCP region).

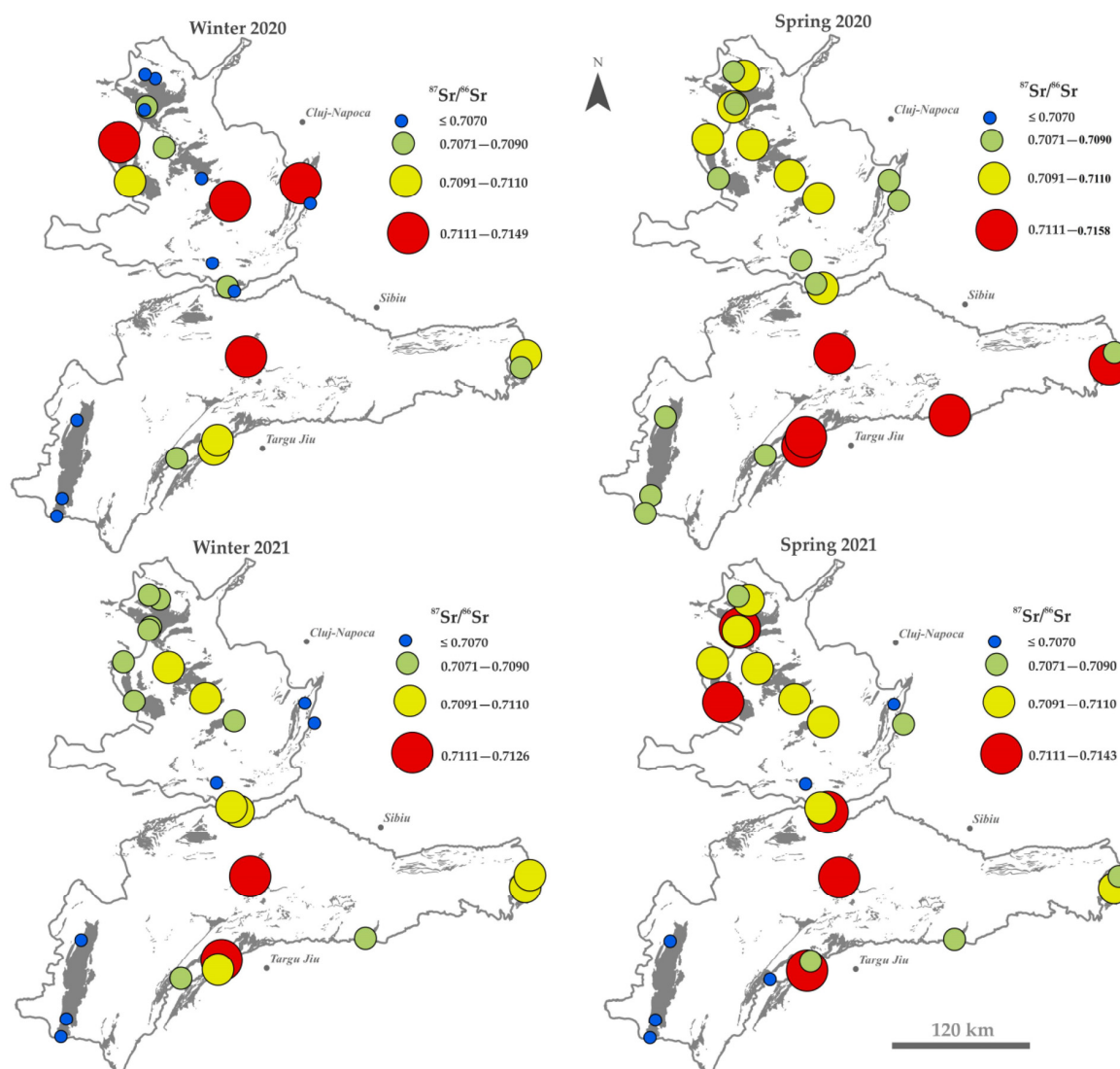


**Figure 7.**  $^{87}\text{Sr}/^{86}\text{Sr}$  ratio in the groundwaters from Southern Carpathians (SCP) and Apuseni Mountains (APS) karst areas.

The relationship between the  $\epsilon\text{Sr}$  and  $\text{Mg}/\text{Ca}$  provides information on the sources of the Sr (Figure 9). Generally, Sr originating from silicate rocks has high  $\epsilon\text{Sr}$  values and a medium ratio of Mg and Ca. Sr originating from carbonate rocks has lower  $\epsilon\text{Sr}$  values and a low ratio of Mg and Ca in the case of calcite aquifers, and a high ratio of Mg and Ca in the case of dolomite aquifers [60]. In the present study, most of the groundwater samples were plotted in the transition area between calcite or silicate dissolution, due to the low Mg and Ca ratios. Only GWR18 and GWR19, from the APS region, were plotted in the transition area between the silicates and dolomites, indicating that the Sr concentration in these two samples was derived from the dolomite or silicate dissolution, in both years (Figure 9). There were no significant differences in the relationship between the  $\epsilon\text{Sr}$  and  $\text{Mg}/\text{Ca}$  among the sampling seasons, indicating no external interference in the origin of the Sr, except for carbonate and silicate dissolutions [39].

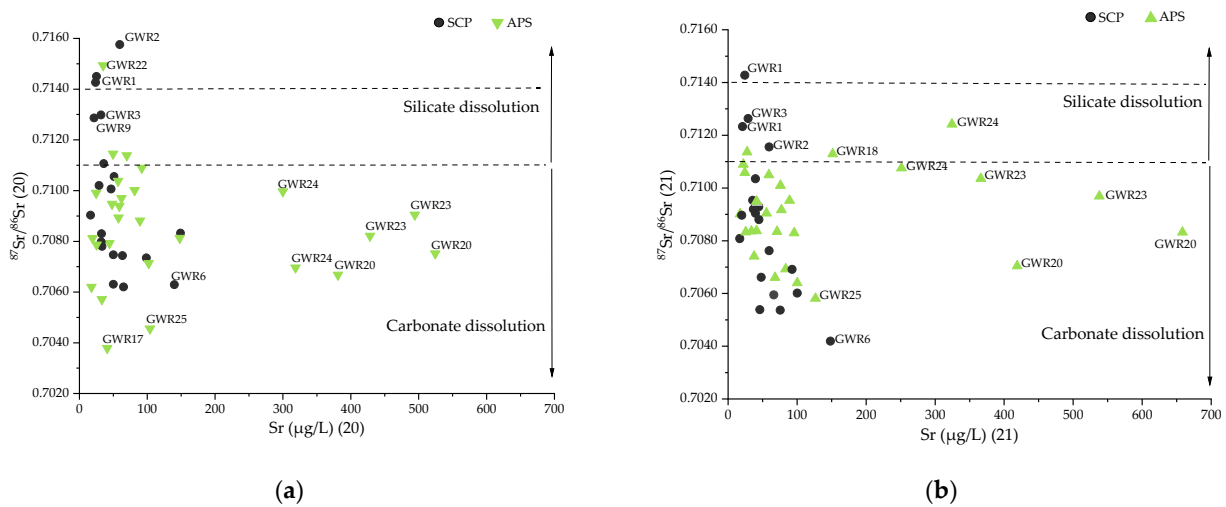


**Figure 8.** The  $^{87}\text{Sr}/^{86}\text{Sr}$  and Sr concentration ( $\mu\text{g}/\text{L}$ ) from the groundwater samples in the year 2020 (a), and 2021 (b).

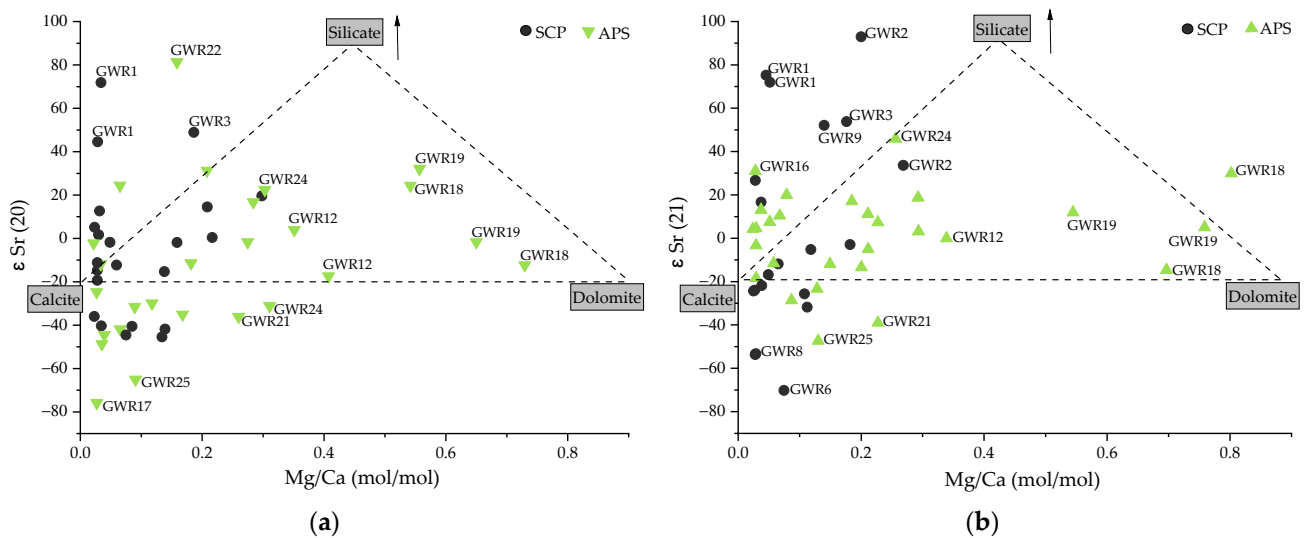


**Figure 9.** Diagram of  $\epsilon\text{Sr}$  vs.  $\text{Mg}/\text{Ca}$  for the groundwater samples in the year 2020 (a), and 2021 (b).

#### 4. Conclusions

The strontium concentrations ranged from 15 to 150  $\mu\text{g}/\text{L}$  in the groundwater samples from the karst areas located in the Southern Carpathians, while higher values were obtained from the Apuseni Mountains, ranging from 17 to 660  $\mu\text{g}/\text{L}$ . Thus, the highest Sr concentrations were measured in the Apuseni Mountains, in the sampling locations GWR20 and GWR23. However, the measured Sr concentrations were below the health reference level of 1500  $\mu\text{g}/\text{L}$ . As the alkali earth elements have similar geochemical behavior to Sr, the higher Sr concentrations in the Apuseni Mountains were correlated with higher Ca, Mg, Li, and Ba concentrations, whereas the results of the molar ratios indicated calcite dissolution over dolomite dissolution. The Sr isotopic signature showed slightly higher  $^{87}\text{Sr}/^{86}\text{Sr}$  ratios and lower Sr concentrations in the groundwaters from the Southern Carpathians compared to the Apuseni Mountains. Therefore, the higher  $^{87}\text{Sr}/^{86}\text{Sr}$  ratios can be associated with silicate dissolution, while the lower  $^{87}\text{Sr}/^{86}\text{Sr}$  ratios with carbonate dissolution. The influence of mineral weathering from the sampling locations had a direct effect on the regional variations of Sr and its isotopic signature. This study presents data on the major and trace element concentrations, as well as on the Sr isotopic signatures, of the groundwaters from two karst areas in Romania. The study had several limitations: (i) there

are no detailed geological data available for the spring areas; (ii) the springs are small and used by local populations, and there are no previous hydrological studies; (iii) the waters were analyzed during two seasons in two consecutive years. To obtain a clearer view of the temporal variations of the Sr isotopic signature, more frequent sampling and event-based measurements would be necessary; (iv) the limited data on the local geochemical setting of the aquifer make it difficult to link the Sr isotopic profile to the type of parent rock that is present in the studied areas; and (v) mass transport simulations should be conducted based on the temporal variability, in order to establish the aquifer recharge influence on the Sr signature.

**Supplementary Materials:** The following supporting information can be downloaded at: <https://www.mdpi.com/article/10.3390/w15071431/s1>, Table S1. Major (Ca, Na, Mg, K) and trace (Sr, Ba, Mn, Li) elements concentration in groundwaters from Southern Carpathians (SCP) and Apuseni Mountains (APS) karst areas, in winter (W) and spring (S) seasons of 2020 and 2021. Table S2. Anions ( $\text{Cl}^-$ ,  $\text{SO}_4^{2-}$ ,  $\text{NO}_3^-$ ,  $\text{HCO}_3^-$ ) concentration, turbidity (TU) and flow rate in groundwaters from Southern Carpathians (SCP) and Apuseni Mountains (APS) karst areas, in winter (W) and spring (S) seasons of 2020 and 2021. Table S3. Ca/Mg, Ca+Mg, Ca/Ca+Mg, Na+K, Ca/Sr, Ba/Sr molar ratio in groundwaters from Southern Carpathians (SCP) and Apuseni Mountains (APS) karst areas, in winter (W) and spring (S) seasons of 2020 and 2021. Table S4.  $^{87}\text{Sr}/^{86}\text{Sr}$  isotopic ratio in the groundwaters from Southern Carpathians (SCP) and Apuseni Mountains (APS) karst areas, in winter (W) and spring (S) seasons of 2020 and 2021.

**Author Contributions:** Conceptualization, A.I.T., E.A.L. and O.T.M.; methodology, C.T., E.A.L. and E.K.; validation, A.I.T., A.M., E.K. and C.T.; investigation, A.I.T., A.M., E.A.L., C.T., I.C.M. and E.K.; visualization, A.I.T. and I.C.M.; writing—original draft preparation, A.I.T., A.M., E.K., E.A.L. and C.T.; writing—review and editing, A.I.T., E.K., E.A.L., I.C.M. and O.T.M.; funding acquisition, O.T.M. All authors have read and agreed to the published version of the manuscript.

**Funding:** This work was supported by the Romanian Ministry of Research and Innovation, CCCDI-UEFISCDI, through projects 352PED/2020 (GLAZEX) and PN-III-P4-ID-PCCF-2016-0016-P (2/2019, DARKFOOD) and by EEA Financial Mechanism 2014–2021 under the project EEA-RO-NO-2018-0138 (GROUNDWATERISK), contract No. 4/2019. The APC was funded by the Romanian Ministry of Research and Innovation, CCCDI-UEFISCDI, through project PN-III-P4-ID-PCCF-2016-0016 (DARKFOOD).

**Data Availability Statement:** The data presented in this study are available upon request from the corresponding author.

**Acknowledgments:** The authors are grateful to Marius Kenesz, Traian Brad, Răzvan Arghir and Alexandru Petculescu for the help with the sampling.

**Conflicts of Interest:** The authors declare no conflict of interest. The funders had no role in the design of the study; in the collection, analyses, or interpretation of data; in the writing of the manuscript; or in the decision to publish the results.

## References

1. Stevanović, Z. Karst waters in potable water supply: A global scale overview. *Environ. Earth Sci.* **2019**, *78*, 662. [CrossRef]
2. Tsakiris, G.; Alexakis, D. Karstic spring water quality: The effect of groundwater abstraction from the recharge area. *Desalination Water Treat.* **2014**, *52*, 2494–2501. [CrossRef]
3. Brad, T.; Bizic, M.; Ionescu, D.; Chiriac, C.M.; Kenesz, M.; Roba, C.; Ionescu, A.; Fekete, A.; Mirea, I.C.; Moldovan, O.T. Potential for natural attenuation of domestic and agricultural pollution in karst groundwater environments. *Water* **2022**, *14*, 1597. [CrossRef]
4. Condon, L.E.; Maxwell, R.M. Evaluating the relationship between topography and groundwater using outputs from a continental-scale integrated hydrology model. *Water Resour. Res.* **2015**, *51*, 6602–6621. [CrossRef]
5. Tóth, J. A theoretical analysis of groundwater flow in small drainage basins. *J. Geophys. Res.* **1963**, *68*, 4795–4812. [CrossRef]
6. Devito, K.; Creed, I.; Gan, T.; Mendoza, C.; Petrone, R.; Silins, U.; Smerdon, B. A framework for broad-scale classification of hydrologic response units on the Boreal Plain: Is topography the last thing to consider? *Hydrol. Process.* **2005**, *19*, 1705–1714. [CrossRef]
7. Haitjema, H.M.; Mitchell-Bruker, S. Are water tables a subdued replica of the topography? *Ground Water* **2005**, *43*, 781–786. [CrossRef]
8. Wood, W.W.; Smedley, P.L.; Lindsey, B.D.; Wood, W.T.; Kirchheim, R.E.; Cherry, J.A. Global Groundwater Solute Composition and Concentrations. *Ground Water* **2022**, *60*, 714–720. [CrossRef]
9. Zhang, Z.; Chen, X.; Soulsby, C. Catchment-scale conceptual modelling of water and solute transport in the dual flow system of the karst critical zone. *Hydrol. Process.* **2017**, *31*, 3421–3436. [CrossRef]

10. Gong, X.; Weng, B.; Yan, D.; Yang, Y.; Yan, D.; Niu, Y.; Wang, H. Potential recharge sources and origin of solutes in groundwater in the central Qinghai–Tibet Plateau using hydrochemistry and isotopic data. *J. Hydrol. Reg. Stud.* **2022**, *40*, 101001. [[CrossRef](#)]
11. Musgrove, M.; Banner, J.L. Controls on the spatial and temporal variability of vadose dripwater geochemistry: Edwards aquifer, central Texas. *Geochim. Cosmochim. Acta* **2004**, *68*, 1007–1020. [[CrossRef](#)]
12. Liu, H.-C.; You, C.-F.; Zhou, H.; Huang, K.-F.; Chung, C.-H.; Huang, W.-J.; Tang, J. Effect of calcite precipitation on stable strontium isotopic compositions: Insights from riverine and pool waters in a karst cave. *Chem. Geol.* **2017**, *456*, 85–97. [[CrossRef](#)]
13. Capo, R.C.; Stewart, B.W.; Chadwick, O.A. Strontium isotopes as tracers of ecosystem processes: Theory and methods. *Geoderma* **1998**, *82*, 197–225. [[CrossRef](#)]
14. Nebel, O.; Stammeier, J.A. Strontium Isotopes. In *Encyclopedia of Geochemistry: A Comprehensive Reference Source on the Chemistry of the Earth*; White, W.M., Ed.; Springer International Publishing: Cham, Switzerland, 2018; pp. 1379–1384. [[CrossRef](#)]
15. Brennan, S.R.; Fernandez, D.P.; Mackey, G.; Cerling, T.E.; Bataille, C.P.; Bowen, G.J.; Wooller, M.J. Strontium isotope variation and carbonate versus silicate weathering in rivers from across Alaska: Implications for provenance studies. *Chem. Geol.* **2014**, *389*, 167–181. [[CrossRef](#)]
16. Jacobson, A.D.; Wasserburg, G.J. Anhydrite and the Sr isotope evolution of groundwater in a carbonate aquifer. *Chem. Geol.* **2005**, *214*, 331–350. [[CrossRef](#)]
17. Salifu, M.; Aiglsperger, T.; Hällström, L.; Martinsson, O.; Billström, K.; Ingri, J.; Dold, B.; Alakangas, L. Strontium ( $^{87}\text{Sr}/^{86}\text{Sr}$ ) isotopes: A tracer for geochemical processes in mineralogically-complex mine wastes. *Appl. Geochem.* **2018**, *99*, 42–54. [[CrossRef](#)]
18. Wang, Y.; Guo, Q.; Su, C.; Ma, T. Strontium isotope characterization and major ion geochemistry of karst water flow, Shentou, northern China. *J. Hydrol.* **2006**, *328*, 592–603. [[CrossRef](#)]
19. Nakano, T. Potential uses of stable isotope ratios of Sr, Nd, and Pb in geological materials for environmental studies. *Proc. Jpn. Acad. Ser. B* **2016**, *92*, 167–184. [[CrossRef](#)]
20. Faure, G.; Mensing, T.M. *Isotopes: Principles and Applications*; Wiley: Delhi, India, 2009.
21. Khaska, M.; Le Gal La Salle, C.; Lancelot, J.; Team, A.; Mohamad, A.; Verdoux, P.; Noret, A.; Simler, R. Origin of groundwater salinity (current seawater vs. saline deep water) in a coastal karst aquifer based on Sr and Cl isotopes. Case study of the La Clape massif (southern France). *Appl. Geochem.* **2013**, *37*, 212–227. [[CrossRef](#)]
22. Blum, J.D.; Erel, Y. 5.12-Radiogenic Isotopes in Weathering and Hydrology. In *Treatise on Geochemistry*; Holland, H.D., Turekian, K.K., Eds.; Pergamon: Oxford, UK, 2003; pp. 365–392. [[CrossRef](#)]
23. Nwankwo, C.B.; Hoque, M.A.; Islam, M.A.; Dewan, A. Groundwater constituents and trace elements in the basement aquifers of Africa and sedimentary aquifers of Asia: Medical hydrogeology of drinking water minerals and toxicants. *Earth Syst. Environ.* **2020**, *4*, 369–384. [[CrossRef](#)]
24. Pu, J.; Yuan, D.; Zhang, C.; Zhao, H. Tracing the sources of strontium in karst groundwater in Chongqing, China: A combined hydrogeochemical approach and strontium isotope. *Environ. Earth Sci.* **2012**, *67*, 2371–2381. [[CrossRef](#)]
25. Jiang, Y. Strontium isotope geochemistry of groundwater affected by human activities in Nandong underground river system, China. *Appl. Geochem.* **2011**, *26*, 371–379. [[CrossRef](#)]
26. Calligaris, C.; Mezga, K.; Slejko, F.F.; Urbanc, J.; Zini, L. Groundwater characterization by means of conservative ( $\delta^{18}\text{O}$  and  $\delta^2\text{H}$ ) and non-conservative ( $^{87}\text{Sr}/^{86}\text{Sr}$ ) isotopic values: The classical karst region aquifer case (Italy–Slovenia). *Geosciences* **2018**, *8*, 321. [[CrossRef](#)]
27. McKay, J.; Lenczewski, M.; Leal-Bautista, R.M. Characterization of flowpath using geochemistry and  $^{87}\text{Sr}/^{86}\text{Sr}$  isotope ratios in the Yalahau region, Yucatan Peninsula, Mexico. *Water* **2020**, *12*, 2587. [[CrossRef](#)]
28. Charlier, J.-B.; Bertrand, C.; Mudry, J. Conceptual hydrogeological model of flow and transport of dissolved organic carbon in a small Jura karst system. *J. Hydrol.* **2012**, *460–461*, 52–64. [[CrossRef](#)]
29. Frost, C.D.; Toner, R.N. Strontium isotopic identification of water-rock interaction and ground water mixing. *Ground Water* **2004**, *42*, 418–432. [[CrossRef](#)]
30. Bicalho, C.C.; Batiot-Guilhe, C.; Taupin, J.D.; Patris, N.; Van Exter, S.; Jourde, H. A conceptual model for groundwater circulation using isotopes and geochemical tracers coupled with hydrodynamics: A case study of the Lez karst system, France. *Chem. Geol.* **2019**, *528*, 118442. [[CrossRef](#)]
31. Onac, B.P.; Goran, C. Karst and Caves of Romania: A Brief Overview. In *Cave and Karst Systems of Romania*; Ponta, G.M.L., Onac, B.P., Eds.; Springer International Publishing: Cham, Switzerland, 2019; pp. 21–35. [[CrossRef](#)]
32. Orășeanu, I. *Hidrogeologia Carstului din Munții Apuseni*, 2nd ed.; Belvedere Printig House: Oradea, Romania, 2020.
33. Goran, C.; Constantin, S.; Horoi, V. *Karst Areas in the Southern Carpathians between Cerna and Olt Rivers*; AGIR Publishing House: Bucharest, Romania, 2006; pp. 41–77. [[CrossRef](#)]
34. Hoaghia, M.-A.; Moldovan, A.; Kovacs, E.; Mirea, I.C.; Kenesz, M.; Brad, T.; Cadar, O.; Micle, V.; Levei, E.A.; Moldovan, O.T. Water quality and hydrogeochemical characteristics of some karst water sources in Apuseni Mountains, Romania. *Water* **2021**, *13*, 857. [[CrossRef](#)]
35. Moldovan, A.; Hoaghia, M.-A.; Kovacs, E.; Mirea, I.C.; Kenesz, M.; Arghir, R.A.; Petculescu, A.; Levei, E.A.; Moldovan, O.T. Quality and health risk assessment associated with water consumption—A case study on karstic springs. *Water* **2020**, *12*, 3510. [[CrossRef](#)]
36. Torok, A.I.; Levei, E.A.; Constantin, S.; Moldovan, O.T.; Senila, M.; Cadar, O.; Casoni, D.; Angyus, S.B.; Tanaselia, C.; Covaci, E.; et al. Application of inductively coupled plasma spectrometric techniques and multivariate statistical analysis in the hydrogeochemical profiling of caves—Case study Cloșani, Romania. *Molecules* **2021**, *26*, 6788. [[CrossRef](#)]

37. ISO. *ISO/IEC Guide 98-3:2008 Uncertainty of Measurement-Part 3: Guide to the Expression of Uncertainty in Measurement*; ISO: Geneva, Switzerland, 2008.
38. Kutscher, D.; Nelms, S.; Lofthouse, S.; Ducos, S. Effective Removal of Isobaric Interferences on Strontium and Lead Using Triple Quadrupole ICP-MS. Available online: <https://assets.thermofisher.com/TFS-Assets/CMD/Application-Notes/an-44365-icp-ms-sr-pb-geological-materials-rocks-an44365-en.pdf> (accessed on 19 July 2022).
39. He, X.; Li, P.; Shi, H.; Xiao, Y.; Guo, Y.; Zhao, H. Identifying strontium sources of flowback fluid and groundwater pollution using  $^{87}\text{Sr}/^{86}\text{Sr}$  and geochemical model in Sulige gasfield, China. *Chemosphere* **2022**, *306*, 135594. [[CrossRef](#)] [[PubMed](#)]
40. Chapman, E.C.; Capo, R.C.; Stewart, B.W.; Kirby, C.S.; Hammack, R.W.; Schroeder, K.T.; Edenborn, H.M. Geochemical and strontium isotope characterization of produced waters from marcellus shale natural gas extraction. *Environ. Sci. Technol.* **2012**, *46*, 3545–3553. [[CrossRef](#)] [[PubMed](#)]
41. Environmental Protection Agency. Announcement of Preliminary Regulatory Determinations for Contaminants on the Third Drinking Water Contaminant Candidate List. 2014. Available online: <https://www.federalregister.gov/documents/2014/10/20/2014-24582/announcement-of-preliminary-regulatory-determinations-for-contaminants-on-the-third-drinking-water> (accessed on 15 January 2023).
42. Négrel, P.; Casanova, J.; Aranyosy, J.-F. Strontium isotope systematics used to decipher the origin of groundwaters sampled from granitoids: The Vienne Case (France). *Chem. Geol.* **2001**, *177*, 287–308. [[CrossRef](#)]
43. Lee, S.-G.; Kim, T.-K.; Lee, T.J. Strontium isotope geochemistry and its geochemical implication from hot spring waters in South Korea. *J. Volcanol. Geotherm. Res.* **2011**, *208*, 12–22. [[CrossRef](#)]
44. Gao, J.; Zou, C.; Li, W.; Ni, Y.; Liao, F.; Yao, L.; Sui, J.; Vengosh, A. Hydrochemistry of flowback water from Changning shale gas field and associated shallow groundwater in southern Sichuan Basin, China: Implications for the possible impact of shale gas development on groundwater quality. *Sci. Total Environ.* **2020**, *713*, 136591. [[CrossRef](#)] [[PubMed](#)]
45. Musgrove, M. The occurrence and distribution of strontium in U.S. groundwater. *Appl. Geochem.* **2021**, *126*, 104867. [[CrossRef](#)]
46. Jebreen, H.; Banning, A.; Wohnlich, S.; Niedermayr, A.; Ghanem, M.; Wisotzky, F. The Influence of karst aquifer mineralogy and geochemistry on groundwater characteristics: West Bank, Palestine. *Water* **2018**, *10*, 1829. [[CrossRef](#)]
47. Keesari, T.; Sabarathinam, C.; Sinha, U.K.; Pethaperumal, R.T.; Kamaraj, P. Fate and transport of strontium in groundwater from a layered sedimentary aquifer system. *Chemosphere* **2022**, *307*, 136015. [[CrossRef](#)]
48. FOREGS-EuroGeoSurveys Geochemical Baseline Database, Strontium Stream Water. Available online: [http://weppi.gtk.fi/publ/foregsatlas/maps/Water/w\\_icpoes\\_sr\\_edit.pdf](http://weppi.gtk.fi/publ/foregsatlas/maps/Water/w_icpoes_sr_edit.pdf) (accessed on 30 July 2022).
49. Frei, R.; Frei, K.M.; Kristiansen, S.M.; Jessen, S.; Schullehner, J.; Hansen, B. The link between surface water and groundwater-based drinking water—Strontium isotope spatial distribution patterns and their relationships to Danish sediments. *Appl. Geochem.* **2020**, *121*, 104698. [[CrossRef](#)]
50. Ma, R.; Wang, Y.; Sun, Z.; Zheng, C.; Ma, T.; Prommer, H. Geochemical evolution of groundwater in carbonate aquifers in Taiyuan, northern China. *Appl. Geochem.* **2011**, *26*, 884–897. [[CrossRef](#)]
51. Gonnee, M.E.; Charette, M.A.; Liu, Q.; Herrera-Silveira, J.A.; Morales-Ojeda, S.M. Trace element geochemistry of groundwater in a karst subterranean estuary (Yucatan Peninsula, Mexico). *Geochim. Cosmochim. Acta* **2014**, *132*, 31–49. [[CrossRef](#)]
52. Directive (EU) 2020/2184 of the European Parliament and of the Council of 16 December 2020 on the Quality of Water Intended for Human Consumption (Recast). Available online: <https://eur-lex.europa.eu/legal-content/EN/TXT/PDF/?uri=CELEX:32020L2184&from=EN> (accessed on 14 February 2023).
53. Joodavi, A.; Aghlmand, R.; Podgorski, J.; Dehbandi, R.; Abbasi, A. Characterization, geostatistical modeling and health risk assessment of potentially toxic elements in groundwater resources of northeastern Iran. *J. Hydrol. Reg. Stud.* **2021**, *37*, 100885. [[CrossRef](#)]
54. Chen, Z.; Auler, A.S.; Bakalowicz, M.; Drew, D.; Griger, F.; Hartmann, J.; Jiang, G.; Moosdorf, N.; Richts, A.; Stevanovic, Z.; et al. The World Karst Aquifer Mapping project: Concept, mapping procedure and map of Europe. *Hydrogeol. J.* **2017**, *25*, 771–785. [[CrossRef](#)]
55. Hartmann, A. The hydrology of groundwater systems—From recharge to discharge. *Encycl. Inland Waters Second. Ed.* **2022**, *3*, 324–330. [[CrossRef](#)]
56. Bhat, N.A.; Jeelani, G.; Bhat, M.Y. Hydrogeochemical assessment of groundwater in karst environments, Bringi watershed, Kashmir Himalayas, India. *Curr. Sci.* **2014**, *106*, 1000–1007.
57. Taherian, P.; Joodavi, A. Hydrogeochemical characteristics and source identification of salinity in groundwater resources in an arid plain, northeast of Iran: Implication for drinking and irrigation purposes. *Acque Sotter. Ital. J. Groundw.* **2021**, *10*, 21–31. [[CrossRef](#)]
58. Petelet-Giraud, E.; Luck, J.-M.; Ben Othman, D.; Joseph, C.; Négrel, P. Chemical and isotopic fingerprinting of small ungauged watershed: How far the hydrological functioning can be understood? *Comptes Rendus Geosci.* **2016**, *348*, 379–386. [[CrossRef](#)]
59. Wu, C.; Wu, X.; Mu, W.; Zhu, G. Using isotopes (H, O, and Sr) and major ions to identify hydrogeochemical characteristics of groundwater in the Hongjiannao Lake basin, northwest China. *Water* **2020**, *12*, 1467. [[CrossRef](#)]
60. Sun, J.; Takahashi, Y.; Strosnider, W.H.J.; Kogure, T.; Wang, B.; Wu, P.; Zhu, L.; Dong, Z. Identification and quantification of contributions to karst groundwater using a triple stable isotope labeling and mass balance model. *Chemosphere* **2021**, *263*, 127946. [[CrossRef](#)]



61. Santoni, S.; Huneau, F.; Garel, E.; Aquilina, L.; Vergnaud-Ayraud, V.; Labasque, T.; Celle-Jeanton, H. Strontium isotopes as tracers of water-rocks interactions, mixing processes and residence time indicator of groundwater within the granite-carbonate coastal aquifer of Bonifacio (Corsica, France). *Sci. Total Environ.* **2016**, *573*, 233–246. [[CrossRef](#)]
62. Bakari, S.S.; Aagaard, P.; Vogt, R.D.; Ruden, F.; Johansen, I.; Vuai, S.A. Strontium isotopes as tracers for quantifying mixing of groundwater in the alluvial plain of a coastal watershed, south-eastern Tanzania. *J. Geochem. Explor.* **2013**, *130*, 1–14. [[CrossRef](#)]
63. Akoglu, H. User's guide to correlation coefficients. *Turk. J. Emerg. Med.* **2018**, *18*, 91–93. [[CrossRef](#)] [[PubMed](#)]

**Disclaimer/Publisher's Note:** The statements, opinions and data contained in all publications are solely those of the individual author(s) and contributor(s) and not of MDPI and/or the editor(s). MDPI and/or the editor(s) disclaim responsibility for any injury to people or property resulting from any ideas, methods, instructions or products referred to in the content.